Eclética Química Journal

Original article
iq.unesp.br/ecletica

| Vol. 43 | n. 2 | 2018 |

Incorporation of $CdFe_2O_4$-SiO_2 nanoparticles in $SbPO_4$-ZnO-PbO glasses by melt-quenching process

Juliane Resges Orives[1], Wesley R. Viali[1], Marina Magnani[1], Marcelo Nalin[1]

[1] São Paulo State University (Unesp), Institute of Chemistry, 55 Prof. Francisco Degni St, Araraquara, São Paulo, Brazil

[+] Corresponding author: Juliane Resges Orives, e-mail address: juliane_resges@hotmail.com

ARTICLE INFO

Article history:
Received: March 20, 2018
Accepted: August 14, 2018
Published: August 23, 2018

Keywords:
1. antimony based glass
2. cadmium ferrite nanoparticles
3. optical properties
4. structural properties

ABSTRACT: The development of glasses containing nanoparticles dispersed homogeneously with controlled size and optimum parameters for functionality is a big challenge. In the present work, the ternary system $60SbPO_4$-$30ZnO$-$10PbO$ containing $CdFe_2O_4$-SiO_2 nanoparticles was studied. $CdFe_2O_4$ nanoparticles, with average size of 3.9 nm, were synthesized using the coprecipitation method and, in a second step, protected by a silica layer. Different mass percentages of nanoparticles were mixed to the glass precursors and then transformed into glasses by melt-quenching method. Thermal and structural properties were evaluated by differential scanning calorimetry, Raman spectroscopy, scanning electronic microscopy and transmission electron microscopy. While the optical properties were studied by M-Lines spectroscopy and UV-Vis spectroscopy. The glasses obtained were completely transparent, with yellow color and showed no sign of crystallization according to the techniques used. Scanning and transmission electron microscopy confirm that the methodology used for the incorporation of nanoparticles was efficient. The methodology used to protect the nanoparticles prior to incorporate them to glasses, strongly contributes towards the development of new functional glasses useful for magneto-optics devices.

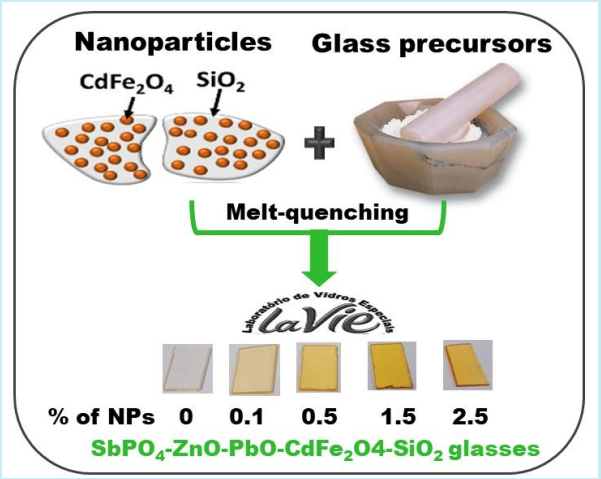

1. Introduction

Antimony phosphate glasses containing heavy metal oxides[1, 2] have been studied due to their interesting characteristics like high linear and non-linear refractive indexes[3, 4], large transmission window[5], low phonon energy[6, 7], which make them promising materials for several technological applications in photonics[8-10] and plasmonics[11, 12].

Another emerging field is related to nanophotonic technologies by incorporating metal, semiconductor or magnetic nanoparticles into such dielectric materials and further to study using femtosecond lasers, in order to understand the fundamental properties of the interaction of light with this new kind of materials[13-18].

How it is a very new field it should be noted that several fundamental aspects must be considered, as for example, what size range of nanoparticles can lead to satisfactory results, what is the amount of nanoparticles supported without crystallizes and what is the influence of the glass matrix nature on the properties of the nanoparticles.

In the case of glasses containing magnetic nanoparticles, the functionality of magneto-optical devices and magnetic sensors can be greatly

improved, but the development of magnetic glasses with nanoparticles dispersed satisfactorily remains a major challenge[19, 20].

For this reason, finding high refractive index matrices that are good hosts for magnetic nanoparticles is important. Despite intensive efforts to study antimony-based glasses, to our knowledge, there is no studies in the literature dedicated to the incorporation of magnetic nanoparticles in these glasses.

The melt-quenching process for the incorporation of nanoparticles has been reported in the literature[20-24], by mixing the glass precursors and nanoparticles powders before melting the material. As the melting process occurs at high temperatures, it is interesting to protect the nanoparticles to ensure that they do not dissolve after the process.

Cadmium ferrite nanoparticles ($CdFe_2O_4$) have been studied due to excellent chemical stability and applicability in magneto-optical devices and semiconductor sensors[25-28]. These nanoparticles can be further functionalized by adding layers of silica, which can act as a protective layer of the nanoparticles during the melting[29-31].

In this context, the proposal of this work was to incorporate cadmium ferrite nanoparticles, synthetized by co-precipitation and coated with silica ($CdFe_2O_4$-SiO_2) into the glass composition $60SbPO_4$-30ZnO-10PbO using the melt-quenching technique. A structural, thermal and optical investigations were performed in the glasses containing the nanoparticles by means of, transmission electron microscopy (TEM), scanning electronic microscopy (SEM), atomic force microscopy (AFM), Raman spectroscopy, differential scanning calorimeter (DSC), M-Lines spectroscopy and UV-Vis spectroscopy.

2. Experimental

2.1 Synthesis of cadmium ferrite nanoparticles protected by a silica layer (CdSiNPs)

The $CdFe_2O_4$ nanoparticles were synthesized by the coprecipitation method, using equal volumes (62.5 mL) of a 0.005 mol L^{-1} solution of cadmium nitrate tetrahydrate (Sigma-Aldrich 99%) and 0.01 mol L^{-1} solution of iron nitrate nonahydrate (Sigma-Aldrich 99%). Then, under stirring, 125 mL of a 1 mol L^{-1} solution of sodium hydroxide (P.A. Synth) was added slowly. The system was kept under a N_2 atmosphere at a controlled heating rate of 10 °C min^{-1} up to 100 °C and was maintained at this temperature for 2 h to complete the reaction. The nanoparticles were washed and then dispersed using ultrasound in 250 mL of ethanol 99%. Subsequently, 3.6 mL of tetraethylorthosilicate (TEOS) (Sigma-Aldrich) and 1.3 mL of 25% ammonium hydroxide solution (P.A Synth) were added in the dispersion of the nanoparticles. The system remained under mechanical stirring for 24 h under N_2 atmosphere. Then, a heat treatment at 600 °C, at room atmosphere, for 5 h was performed to eliminate any organic residue.

2.2 $SbPO_4$-PbO-ZnO glasses (SPZ) containing CdSiNPs

Glass samples were prepared by melt-quenching process. The precursors used in the glass preparation for the $60SbPO_4$-30PbO-10ZnO system were $SbPO_4$ (prepared as reported previously by Nalin *et al.*[32]), PbO and ZnO (grade purity 99%). A sample without nanoparticles (SPZ) and four samples containing 0.1, 0.5, 1.0 and 2.5% in mass of CdSiNPs (SPZ-0.1CdSiNPs, SPZ-0.5CdSiNPs, SPZ-1.0CdSiNPs and SPZ-2.5CdSiNPs) were prepared. The glass composition was weighed (sufficient to prepare 25 g of glass) and subsequently homogenized using an agate mortar. The powder mixture was transferred to a Pt-Au crucible and melted in a furnace at 1100 °C for 30 min. Later, the melt was poured into a brass mold and crushed. The mother glass was separated into 5 portions of 5 g each one and then, the different percentages of nanoparticles (0, 0.1, 0.5, 1.5, 2.5) were mixed. The melting process was repeated for the 5 samples at 1100 °C for 7 min and poured in a brass mold heated at 340 °C and left at such temperature for 2 h for annealing. This procedure is used to eliminate the internal residual stresses of the glass, resulted from the rapid cooling of the liquid and aims to increase the mechanical resistance. The finishing of the samples was obtained by polishing the glasses with SiC sandpaper with different grades. Figure 1a illustrates the silica modification of cadmium ferrite nanoparticles and Figures 1b and c the preparation of glasses by melt-quenching process.

Eclética Química Journal, vol. 43, n. 2, 2018, 32-43
ISSN: 1678-4618
DOI: 10.26850/1678-4618eqj.v43.2.2018.p32-43

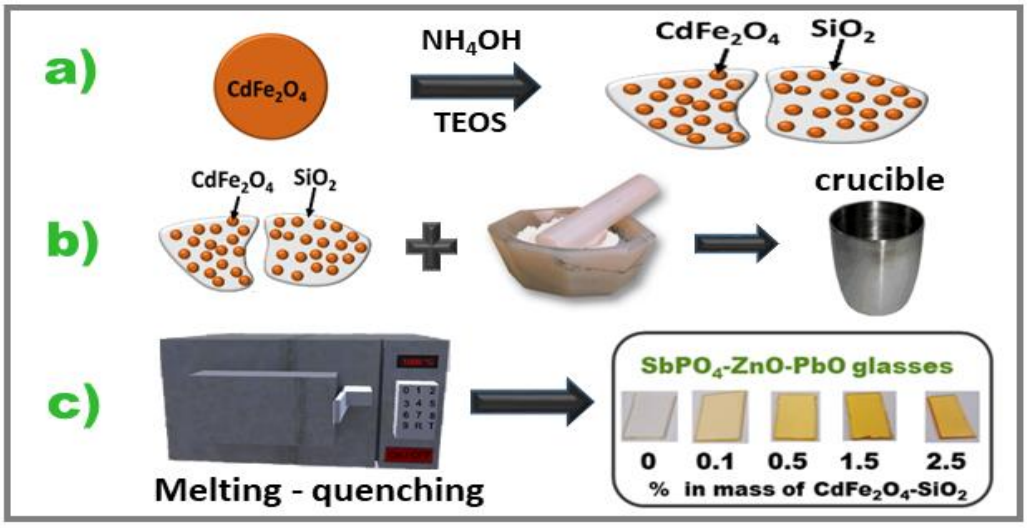

Figure 1. Illustration of: a) silica modification of $CdFe_2O_4$, b) mixture of nanoparticles and glass precursors and c) preparation of glasses containing nanoparticles.

2.3 Nanoparticles and glasses characterization

X-ray powder diffraction were carried out for the CdSiNPs with a Bruker D8 Advance diffractometer operating with a Ni filtered CuKα radiation source at 2θ angle ranging from 10 to 80 ° with a step pass of 0.02 ° and a step time of 2 s. Transmission electron microscopy TEM were carried out using a Philips CM200 equipment operating at 200 kV and equipped with X-ray energy dispersive spectroscopy (EDS) Bruker model XFlash 6TI30. Samples were prepared using 0.1 mg of CdSiNPs or SPZ samples containing CdSiNPs. After grounding, the powder was dispersed in 1 mL of isopropyl alcohol using ultrasound. Some drops of this suspension were applied on a copper grid coated with carbon film. Reflectance spectrum for the CdSiNPs and transmission spectra (in the spectral range from 200 to 800 nm) for the SPZ-CdSiNPs glasses were recorded using a Varian Cary 5000 UV-Vis-Near infrared (NIR) spectrophotometer from the polished samples with 2 mm in thickness. Scanning electron microscopy images were obtained in a high-resolution Scanning Electron Microscope (SEM-FEG HR) – FEI Inspect F50 equipped with *Energy Dispersive* X-ray Spectroscopy (EDS) Probe (Inca Energy-Oxford) in the bulk sample covered with carbon film and in the powder dispersed in isopropyl alcohol by dripping the suspension onto a silicon substrate. Topography images of $SbPO_4$-PbO-ZnO glasses (SPZ) containing CdSiNPs were obtained using a Park NX-10 Atomic Force Microscope. PPP-MFM probes (NanoWorld) with spring constant of 2.8 N/m and resonance frequency within 75 kHz were used for measurements. Topography were acquired in air by single pass scanning at room temperature and humidity between 74.5 and 75.5%. Topography was measured using the intermittent contact mode setup, slightly below the frequency of resonance. Analysis and processing of the AFM images were carried out with Gwyddion[33]. Raman scattering spectra were recorded at room temperature in a frequency range from 200 to 1150 cm^{-1} in a HORIBA Jobin Yvon model LabRAM HR micro Raman apparatus equipped with a 632.8 nm laser, delivering 17 mW. Differential scanning calorimetry (DSC) measurements were carried out using the DSC Q600 equipment from TA Instruments to study the thermal properties of glasses. Small pieces of glasses, with typically 15 mg, were heated in aluminum crucible from 150 to 600 °C at a heating rate of 10 °C.min^{-1}, in N_2 atmosphere (70 mL min^{-1}). The estimated errors are ± 2 °C for T_g and T_x. The refractive index of the samples was measured at 632.8 nm using a Metricon model 2010 equipment. The estimated error is ± 0.0001.

3. Results and discussion

3.1 $CdFe_2O_4$ and CdSiNPs

The X-ray diffraction pattern of the synthesized powder is consistent with a cubic phase of spinel structure (space group: Fd-3m) (Figure 2). The major peak located at 34.4 ° corresponds to the

Eclética Química Journal, vol. 43, n. 2, 2018, 32-43
ISSN: 1678-4618
DOI: 10.26850/1678-4618eqj.v43.2.2018.p32-43

(311) plane which can be readily ascribed to the characteristic peaks of the spinel ferrites. Except for the low intensity diffraction peak at 42.5 ° assigned to the Fe_3O_4 plane (400) according to the standard (JCPDS 19-0629) the remaining diffraction peaks match well with standard (JCPDF 22-1063). The broadening of diffraction peaks indicates the nanocrystalline nature of the synthesized powder[34].

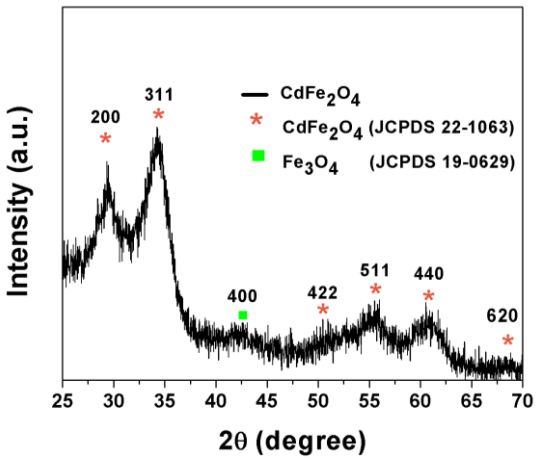

Figure 2. XRD pattern of $CdFe_2O_4$.

A TEM image, obtained for the CdSiNPs, is shown in Figure 3. The upper inset displays the histogram obtained from several TEM images, with size distribution of 3.9 ± 0.1 nm. Moreover, is observed that the nanoparticles present a spherical-like morphology. Plocek *et al.*, prepared nanoparticles of $CdFe_2O_4$@SiO_2, via sol gel methodology, with average size of 3.4 nm, and the TEM profile obtained is very similar to those obtained in this work[29].

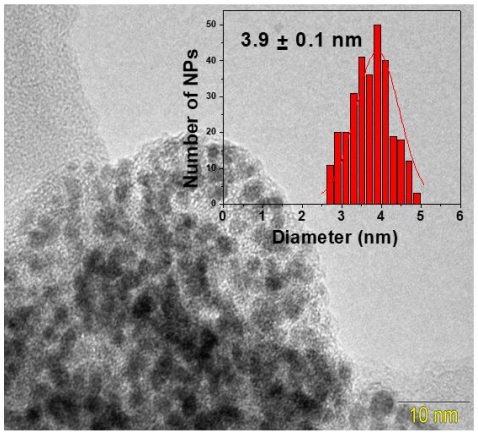

Figure 3. TEM and histogram with the size distribution of CdSiNPs.

The nanoparticles were synthesized by coprecipitation method and was used a surfactant-free synthesis in order to avoid remaining organic compounds, that can induce bubbles during the synthesis of the glass and react with the Pt-Au crucible during the melting process. After coating the CdSiNPs with silica, the nanoparticles were heated at 600 °C for 5 h. For this reason, the nanoparticles are not isolate and monodisperses, but rather in the form of silica agglomerates.

Figure 4a shows the diffuse reflectance spectrum for the CdSiNPs. This technique allows to obtain the band gap energy of the material. The Kubelka-Munk remission function is the most used for interpreting diffuse reflectance data. The absorption coefficient close to the edge of the absorption band is a function of the frequency according to Equation 1:

$$(ahv)^{\frac{1}{n}} = K'.hv - K'.E_{bg} \quad (1)$$

In which K' is the absorption constant that depends on the properties of the material and $h\nu$ is the photon energy of the incident radiation; the exponent n can have values of 1/2, 2, 3/2 and 3 corresponding to direct transition, indirect transition, prohibited direct transition and prohibited indirect transition, respectively[35].

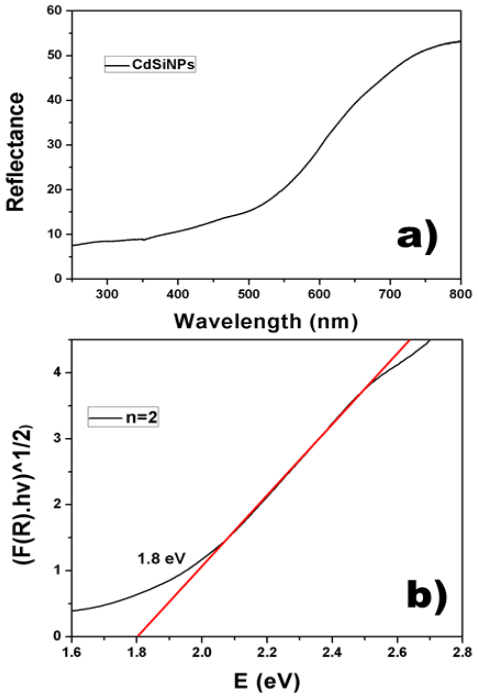

Figure 4. a) Diffuse Reflectance Spectra of CdSiNPs, b) $(F(R).h\nu)^{1/2}$ as a function of the photon energy.

Eclética Química Journal, vol. 43, n. 2, 2018, 32-43
ISSN: 1678-4618
DOI: 10.26850/1678-4618eqj.v43.2.2018.p32-43

The absorption coefficient (a) is related to the reflectance (R) measured by means of Equation 2:

$$a = F(R) \quad (2)$$

where $F(R)$ is the Kubelka-Munk function which has the form expressed in Equation 3:

$$F(R) = (1-R)^2/2R \quad (3)$$

If $F(R).h\nu^{\frac{1}{n}}$ is plotted as a function of the energy of the incident photon and the straight-line portion is extrapolated to $F(R).h\nu^{\frac{1}{n}} = 0$, with n = ½ or 2, the band gap energy can be estimated.

In Figure 4b is shown the graph of $F(R).h\nu^{\frac{1}{n}}$ as a function of photon energy (E) for n=2, which provided lower deviation in the linear regression, the indirect band gap obtained was 1.8 eV. Miao *et al.*[36] calculated an indirect gap for a thin film of $CdFe_2O_4$ of 1.97 eV and Shi *et al.*[37] also obtained a band gap of 1.97 eV for nanoparticles of $CdFe_2O_4$ with 24 nm of diameter. Naseri[28] obtained in his work a band gap of 2.06 eV for nanoparticles with a size of 47 nm treated at 673 °C. Based on these results, and due to the reduced size of the nanoparticles the band gap value obtained is in agreement with the literature.

3.2 SPZ glasses containing CdSiNPs

Figure 1c showed the profile of the matrix and vitreous samples containing nanoparticles obtained. The matrix color is light yellow and when the nanoparticles were incorporated to the samples, they became darker with intensification of the tonality with increasing the percentage of CdSiNPs. The color is characteristic of the presence of iron ions in the glasses[38]. The obtained samples are totally transparent and visually homogeneous. For compositions containing concentrations higher than 3.0% of nanoparticles the total crystallization of the samples occurred, indicating that the limit of nanoparticles supported by the SPZ matrix is between 2.5 and 3.0% in mass of CdSiNPs.

By means of the TEM image of the sample SPZ-2.5CdSiNPs it is seen in Figures 5a and 5b that the sample presents regions with different contrast from the glass without nanoparticles. When these regions were analyzed closely, the presence of the CdSiNPs were confirmed, showing that the incorporation occurred satisfactorily, although it did not occur homogeneously in the nanoscale.

The Figures 5c and 5d were obtained in two different regions in which the nanoparticles present average diameter of 3.5 nm (histogram inserted in Figure 5d, obtained from images 5c and 5d), showing that silica coating was efficient to protect nanoparticles during melting at high temperatures. The smaller size with respect to the nanoparticles prior to incorporation can be explained by the low count number of nanoparticles in the glass, and also due to a possible dissolution of the silica layer at the edges of the agglomerates, consequently causing the dissolution of part of the nanoparticles. In this way, iron ions were dispersed into the matrix and explains the dark yellow color.

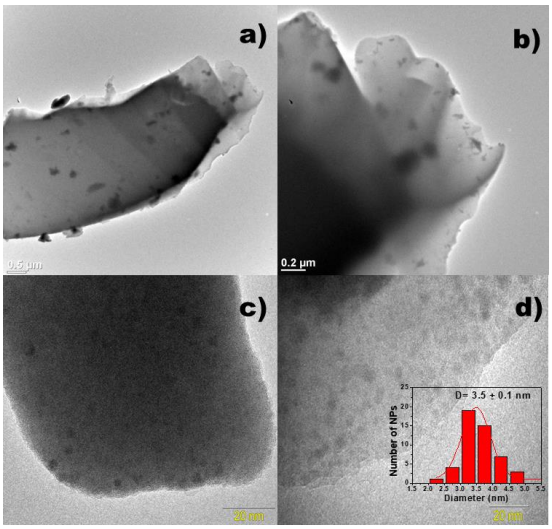

Figure 5. TEM images of SPZ-2.5CdSiNPs sample in different regions: a), b), c) and d). The insert in d) shows the histogram made from TEM images for the sample including images c) and d).

The morphology of the $SbPO_4$-PbO-ZnO glasses (SPZ) containing 2.5% CdSiNPs were studied by SEM and AFM microscopy, Figure 6 and Figure 7, respectively. Figure 6a and 6b displayed silica agglomerates containing $CdFe_2O_4$ nanoparticles with different formats in the glass surface. Figure 6c shows the energy dispersive spectra (EDS) of the general area of Figure 6b. The Cd, Fe, Si peaks were clearly visible in EDS showing the presence of NPs within the glass. The Figure 6d shows the image of a suspension obtained from the sample deposited on a silicon substrate. Agglomerates are observed with different sizes and forms concentrated in certain regions of the sample, and these results are in agreement with the images obtained by TEM.

Eclética Química Journal, vol. 43, n. 2, 2018, 32-43
ISSN: 1678-4618
DOI: 10.26850/1678-4618eqj.v43.2.2018.p32-43

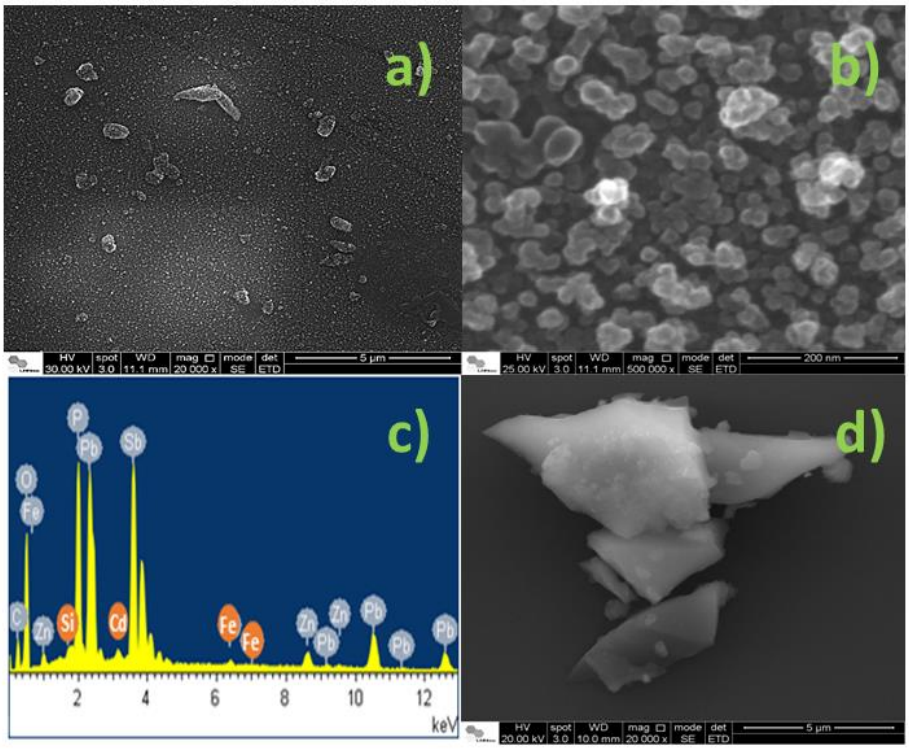

Figure 6. SEM-HR images of SPZ-2.5CdSiNPs sample covered with carbon film a) 20.000x; b) 500.000x, c) EDX spectra of the general area of image (b) and d) SEM-HR image for SPZ-2.5CdSiNPs suspension deposited on silicon substrate (20.000x).

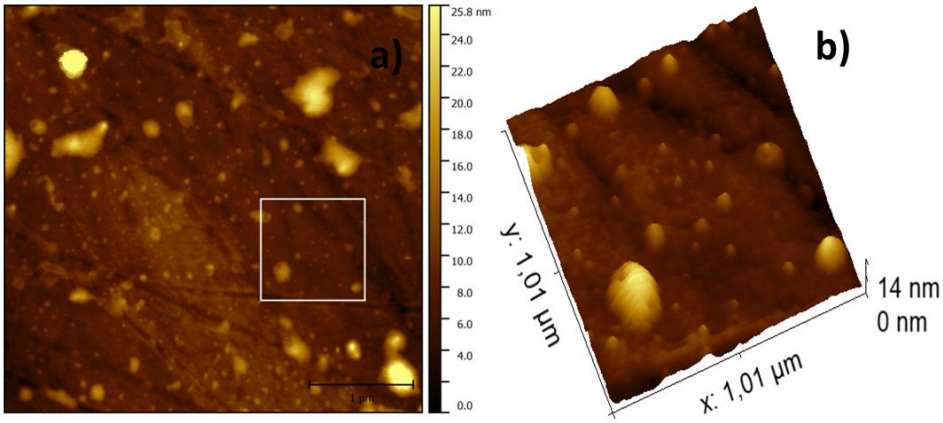

Figure 7. AFM topography images of 4 x 4 μm^2 (*a*) 3D surface topography associated with the region (1 x 1 μm^2) square draw on (*a*).

Figure 7 shows AFM images corresponding to the $SbPO_4$-PbO-ZnO glasses (SPZ) containing 2.5% CdSiNPs. The topography of the SPZ-2.5.0CdSiNPs sample and 3D AFM image clearly reveals the presence of different sizes of agglomerates containing the nanoparticles (30 nm until 0.3 µm) uniformly disperses on glass, corroborating with TEM and SEM images. We assign the presence of the silica agglomerates to the low melting time (7 min), which was not enough to dissolve all the silica in the sample, protecting the nanoparticles.

3.3 Thermal analysis

Figure 8 shows the DSC curves for the matrix and for the samples containing nanoparticles in different percentage in mass. It is observed that the profile of the curves is the same for all samples. The values found for characteristic temperatures of

Eclética Química Journal, vol. 43, n. 2, 2018, 32-43
ISSN: 1678-4618
DOI: 10.26850/1678-4618eqj.v43.2.2018.p32-43

glass transition (T_g), onset of crystallization (T_x) and maximum crystallization (T_p) of each sample are resumed in Table 1. The addition of nanoparticles leads to a small increase in the value of T_g and T_x, attributed to the increase in the degree of structural rigidity due to the incorporation of the silica in the matrix. The parameter T_x-T_g, referring to the thermal stability of the glass, remains constant, showing that the addition of the nanoparticles to the glass did not destabilizes the composition. This behavior is important for applications when glass pieces with different sizes (for example, 10 x 10 cm) are required.

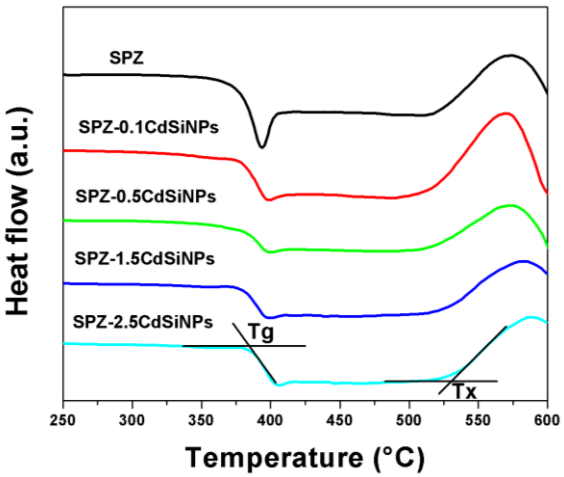

Figure 8. DSC curves of the SPZ and SPZ-CdSiNPs glasses.

Table 1. Characteristic temperatures of the SPZ-CdSiNPs glasses.

Samples	T_g (°C)	T_x (°C)	T_p (°C)	T_x-T_g (°C)
SPZ	375	515	573	140
SPZ-0.1CdSiNPs	379	519	571	140
SPZ-0.5CdSiNPs	380	518	574	138
SPZ-1.5CdSiNPs	381	523	582	142
SPZ-2.5CdSiNPs	385	530	588	145

3.4 Raman Spectroscopy

The prepared samples were analyzed by Raman spectroscopy (Figure 9). Due to the higher proportion of $SbPO_4$ in the glasses studied, the curves predominantly present bands characteristic of the phosphate groups, and can be attributed as published by Nalin *et al.*[4]

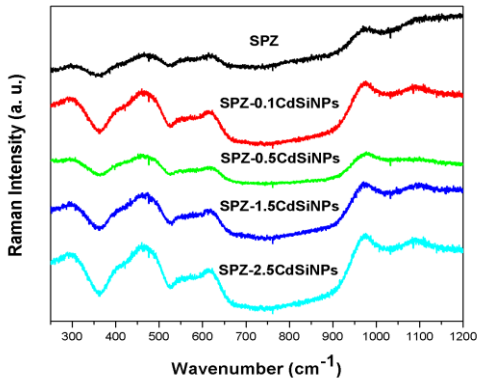

Figure 9. Raman spectra of the SPZ and SPZ-CdSiNPs glasses.

The band at 300 cm^{-1} is assigned to group modes.[1] The bands at 461 and 404 cm^{-1} are assigned to symmetrical deformation of the PO_4 and the asymmetric deformation of Sb-O, respectively. While the bands at 617 and 551 cm^{-1} are assigned to the asymmetrical stretches of vibrational modes P-O-Sb and asymmetrical stretching Sb-O. Finally, the bands at 1100 and 972 cm^{-1} can be assigned to asymmetrical stretches of the PO_4 and symmetrical stretching of PO_4, respectively.

Assignments for samples containing CdSiNPs are shown in Table 2. The positions of the bands remain constant and no evidence that the addition of the nanoparticles is modifying the structure of the glass was found.

Eclética Química Journal, vol. 43, n. 2, 2018, 32-43
ISSN: 1678-4618
DOI: 10.26850/1678-4618eqj.v43.2.2018.p32-43

Table 2. Assignments of the bands observed in the Raman spectrum for the glasses studied.

	Raman/cm^{-1}						
Samples	**G.M.***	**δ_{as} Sb-O**	**δ_s PO_4**	**ν_{as} Sb-O**	**ν_{as} P-O-Sb**	**ν_s PO_4**	**ν_{as} PO_4**
SPZ	300	404	461	546	617	972	1100
SPZ-0.1CdSiNPs	298	404	465	547	617	973	1097
SPZ-0.5CdSiNPs	299	405	467	547	619	972	1098
SPZ-1.5CdSiNPs	300	405	465	547	617	973	1198
SPZ-2.5CdSiNPs	298	405	467	549	619	972	1198

G.M.: Group Modes

3.5 Optical measurements

The refractive index values for glasses were obtained using the prism coupling technique, M-lines spectroscopy and the values can be observed in the Table 3.

The increase in nanoparticle concentration slightly reduced the refractive index, which can be attributed to the contribution of silica and the substitution of PbO and $SbPO_4$ in the matrix, which have much higher polarizabilities, leading to a decrease in refractive index values. While Siqueira[39] found to the same vitreous matrix a behavior of increase of refractive index with increase of the concentration of Fe_2O_3, which was attributed to the ability of iron ions to polarize neighboring atoms.

Table 3. Refractive Indexes obtained for the SPZ and SPZ-CdSiNPs glasses.

Samples	Refractive Index
SPZ	1.887
SPZ-0.1CdSiNPs	1.886
SPZ-0.5CdSiNPs	1.885
SPZ-1.5CdSiNPs	1.883
SPZ-2.5CdSiNPs	1.880

Spectroscopy in the UV-Vis region was used to obtain transmission spectra of the matrix and samples containing CdSiNPs. Figure 10 shows that it occurs a red shift of the absorption edge with the increase in the percentage in mass of CdSiNPs. The decrease of the transmittance is due to light scattering from scratches on the surface of the glasses and also due to the scattering coming from the presence of agglomerates. Higher is the percentage of nanoparticles, higher is the agglomerates and, as consequence, lower is the transmission of the glasses.

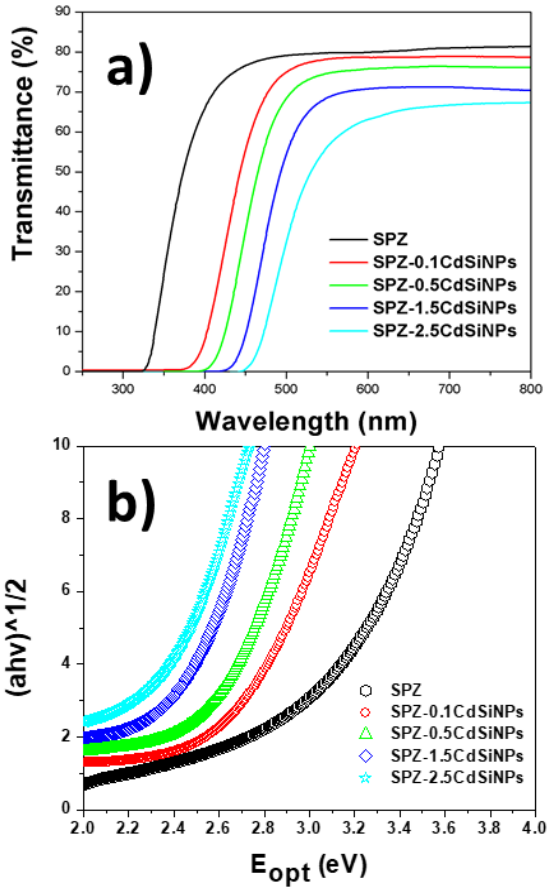

Figure 10. a) Transmittance spectra obtained for the $SbPO_4$-PbO-ZnO containing CdSiNPs and b) $(ah\nu)^{1/2}$ as function of the energy of the photon (E).

The absorption limit in the visible region is called band gap energy and involves optical transitions between the valence and conduction

Eclética Química Journal, vol. 43, n. 2, 2018, 32-43
ISSN: 1678-4618
DOI: 10.26850/1678-4618eqj.v43.2.2018.p32-43

bands. Its value can be obtained from the transmission spectra using the PARAV software in which the transmission spectra of the glasses is inserted and also the values of the refractive indexes and thicknesses of the glasses are supplied to the software, which then generates the graph of $(ah\nu)^{1/2}$ *versus* E[40].

As already mentioned above, the absorption coefficient is a function of the frequency, so plotting a graph of $(ah\nu)^{1/2}$ as a function of the energy of the photon (E), is possible to obtain the band gap energy values of the glasses (Figure 10b).

The Figure 11 shows the values of the optical band gap (E_{opt}) of the glasses (which were determined from a tangent drawn in the intercession of the curve $(ah\nu)^{1/2}$ *versus* E). Band gap energies decrease with increasing percentage in mass of CdSiNPs and it can be attributed to the fact that the nanoparticles and iron ions introduce new energy levels between the valence band and the conduction band of the matrix, showing that E_{opt} the of the SPZ glass is strongly sensitive to the presence of CdSiNPs.

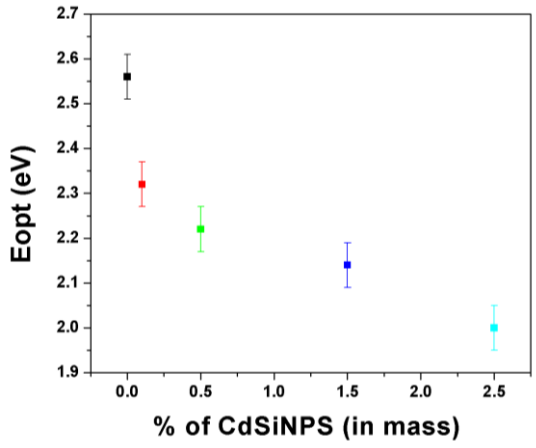

Figure 11. Optical band gap energy values obtained for the SPZ and SPZs containing CdSiNPs.

The results obtained in this work are important from the fundamental point of view because demonstrate the possibility to use glass as a medium to disperse nanoparticles without dissolves them. Glasses containing nanoparticles are interesting system for several applications in photonics, however the nanoparticles usually are growth from the vitreous phase by means of a controlled heat treatment. The main drawback of such method is linked to the fact that most of glasses crystallize heterogeneously leading to non-homogeneous optical properties.

The innovation in this paper is related to the fact that we proved that nanoparticles with controlled sizes can be dispersed into glass matrix. Such results open the possibility to explore new functionalities for such materials in the field of photonics and magneto-photonics. It is important to remember the reader that conventional glasses, like those used for optical fibers, are not suitable to changes in the electromagnetic fields close to them, however, using this new hybrid glasses the magnetic properties of the nanoparticles may play a very interesting role on the manipulation of the light by means of changes in the magnetic field. Applications such as, sensors may be idealized using such new materials. These possibilities are currently under investigation in our laboratory.

4. Conclusion

In this work, the $60SbPO_4$-30ZnO-10PbO glass system was used as host for incorporation of CdSiNPs using melt-quenching process. We have shown that the method of protection of the nanoparticles with a silica layer is efficient and the incorporation in the vitreous matrix occurred satisfactorily, as presented in TEM and SEM images, although it is still necessary to improve the quality of the silica coating in order to obtain monodisperse nanoparticles and more homogeneous glasses. The DSC analysis showed that the matrix acquired greater thermal stability while Raman spectroscopy did not present evidence that the presence of the CdSiNPs modified the glass structure. This is interesting because nanocrystals were added in an amorphous matrix without causing crystallization of the sample. The presence of the nanoparticles induced a decrease in the refractive index and E_{opt} of the glass, showing that the CdSiNPs have influence on the optical properties of the material. The results obtained in this work may contribute towards the development of glasses containing nanoparticles useful for magneto-optics devices. In addition, it is important to emphasize that this methodology can be used for other types of nanoparticles such as bimetallic nanoparticles or nanoparticles with plasmonic properties, for example, thus expanding the range of possibilities of studies in the area of nanoparticles containing glasses.

Eclética Química Journal, vol. 43, n. 2, 2018, 32-43
ISSN: 1678-4618
DOI: 10.26850/1678-4618eqj.v43.2.2018.p32-43

5. Acknowledgements

The authors are grateful to the Brazilian funding agencies CNPq (grant number 141258/2014-4) and São Paulo Research Foundation FAPESP (grant number #2013/07793-6). We would like to thanks LME and LCS -LNNano/CNPEM, which provides the equipments for SEM and AFM measurements.

6. References

[1] Manzan, R. S., Donoso, J. P., Magon, C. J., Silva, I. d'A. A., Rüsseld, C., Nalin, M. Optical and Structural Studies of Mn^{2+} Doped $SbPO_4$-ZnO-PbO Glasses, J. Braz. Chem. Soc. 26 (12) (2015), 2607-2614. https://doi.org/10.5935/0103-5053.20150289.

[2] Franco, D. F., Hssen Fares, H., Souza, A. E., Santagneli, S. H., Nalin, M., Glass formation and the structural study of the Sb2O3-SbPO4-WO3 system, Eclet. Quim. J. 42 (1) (2017) 51-59. https://doi.org/10.26850/1678-4618eqj.v42.1.2017.p51-59.

[3] Falcão Filho, E. L., Bosco, C.A.C., Maciel, G. S., Araujo, C. B., Nalin, M., Messaddeq, Y., Ultrafast nonlinearity of antimony polyphosphate glasses, Appl. Phys. Lett. 83 (2003) 1292-1294. https://doi.org/10.1063/1.1601679.

[4] Volpi, V., Montesso, M., Ribeiro, S. J. L., Viali, W. R., Magon, C. J., Silva, I. D. A., Donoso, J. P., Nalin, M., Optical and structural properties of Mn^{2+} doped $PbGeO_3$-$SbPO_4$ glasses and glass-ceramics, J. Non-Cryst. Sol. 431(2016) 135-139. https://doi.org/10.1039/C8DT00560E.

[5] Moustafa, S.Y., Sahar, M.R., Ghoshal, S.K., Comprehensive thermal and structural characterization of antimony-phosphate glass, Results phys. 7 (2017) 1396-1411. https://doi.org/10.1016/j.rinp.2017.04.006.

[6] Miller, P. J., Cody, C. A., Infrared and Raman investigation of vitreous antimony trioxide, Spectrochim. Acta A-M. 38 (5) (1982) 555-559. https://doi.org/10.1016/0584-8539(82)80146-3.

[7] Nalin, M., Poirier, G., Messaddeq, Y., Ribeiro, S. J. L., Carvalho, E. J., Cescato, L., Characterization of the reversible photoinduced optical changes in Sb-based glasses, J. Non-Cryst. Sol. 352 (2006) 3535-3539. https://doi.org/10.1016/j.jnoncrysol.2006.03.087.

[8] Manzani, D., Montesso, M., Mathias, C. F., Krishanaiah, K. V., Ribeiro, S. J. L., Nalin, M., Visible up-conversion and near-infrared luminescence of Er^{3+}/Yb^{3+} co-doped $SbPO_4$ GeO_2 glasses, Opt. Mater. 57 (2016) 71-78. https://doi.org/10.1016/j.optmat.2016.04.019.

[9] Ouannes, K., Lebbou, K., Walsh, B. M., Poulain, M., Alombert-Gotet, G., Guyot, Y., Antimony oxide based glasses, novel laser materials, Opt. Mater. 65 (2017) 8-14. https://doi.org/10.1016/j.optmat.2016.11.017.

[10] Rao, V. H., Prasad, P. S., Rao, P. V., Santos, L. F., Veeraiah, N., Influence of Sb_2O_3 on tellurite based glasses for photonic applications, J. Alloys Compd. 687 (2016) 898-905. https://doi.org/10.1016/j.jallcom.2016.06.256.

[11] Shasmal, N., Karmakar, B., Tuneable and Au-enhanced yellow emission in Dy^{3+}/Au co-doped antimony oxide glass nanocomposites, J. Non-Crys. Solids. 463 (2017) 40-49. https://doi.org/10.1016/j.jnoncrysol.2017.02.019.

[12] Franco, D. F., Sant'Ana, A. C., Oliveira L. F. C., Silva, M. A. P., The Sb_2O_3 redox route to obtain copper nanoparticles in glasses with plasmonic properties, J. Mater. Chem. C. 3 (2015) 3803-3808. https://doi.org/10.1039/C5TC00102A.

[13] Prasad, P.N. Nanophotonics, Wiley, New Jersey, 2004.

[14] Gonella, F., Mazzoldi, P. Handbook of nanostructured materials and nanotechnology, Academic Press, San Diego v. 4, 2000, ch2.

[15] Sharma, S., Singh, S., Prajapat, C.L., Bhattacharya, S., Preparation and study of magnetic properties of silico phosphate glass and glass-ceramics having iron and zinc oxide, J. Mag. Mag. Mat. 321(22) (2009) 3821-3828. https://doi.org/10.1016/j.jmmm.2009.07.047.

[16] Bigot, J.-Y., Mircea., V., Beaurepaire, E., Coherent ultrafast magnetism induced by femtosecond laser pulses, Nature Phys. 5 (2009) 515-520. https://doi.org/10.1038/nphys1285.

[17] Boeglin, C., Beaurepaire, E., Halté, V., López-Flores, V., Stamm, C., Pontius, N., Dürr , H. A., Bigot, J.-Y. Distinguishing the ultrafast dynamics of spin and orbital moments in solids, Nature. 465 (2010) 458-461. https://doi.org/10.1038/nature09070.

[18] Nakashima, S., Sugioka, K., Tanaka, k., Midorikawa, k., Mukai, k., Optical and magneto-optical properties in Fe-doped glasses irradiated with femtosecond laser, Appl. Phys. B. 113 (3) (2013) 451- 456. https://doi.org/10.1007/s00340-013-5489-z.

[19] Kim, K.D., Kim, S.S., Choa, Y.H., Kim, H.T., Formation and surface modification of Fe_3O_4 nanoparticles by co-precipitation and sol-gel method, J. Ind. Eng. Chem.7 (2007) 1137-1141.

[20] Widanarto, W., Sahar, M.R., Ghoshal, S.K., Arifin, R., Rohani, M.S., Effendi, M., Thermal, structural and magnetic properties of zinc-tellurite glasses containing natural ferrite oxide, Mat. Lett. 108 (2013) 289–292. https://doi.org/10.1016/j.matlet.2013.06.109.

[21] Anigrahawati, P., Sahar, M. R., Ghoshal, S. K., Influence of Fe_3O_4 nanoparticles on structural, optical and magnetic properties of erbium doped zinc phosphate glass, Mater. Chem. Phys. 155 (2015) 155-161. https://doi.org/10.1016/j.matchemphys.2015.02.014.

[22] Widanarto, W., Sahar, M. R., Ghoshal, S. K., Arifin , R., Rohani, M.S., Hamzah, K., Effect of natural Fe_3O_4 nanoparticles on structural and optical properties of Er^{3+} doped tellurite glass, J. Mag. Mag. Mat. 326 (2013) 123-128. https://doi.org/10.1016/j.jmmm.2012.08.042.

[23] Farag, H. K., Marzouk, M. A., Preparation and characterization of nanostructured nickel oxide and its influence on the optical properties of sodium zinc borate glasses J. Mater. Sci: Mater. Electron. 28 (2017) 15480–15487. https://doi.org/10.1007/s10854-017-7435-z.

[24] Chen, Q. Wan, L. Chen, Zhang, Q. M., Effect of Magnetite Nanoparticles Doped Glass with Enhanced Verdet Constant for Magnetic Optical Current Transducer Applications, Adv. Mater. Res. 270 (2011) 13-18. https://doi.org/10.4028/www.scientific.net/AMR.271-273.13.

[25] Lou, X., Liu, S., Shi, D., Chu, M., Ethanol-sensing characteristics of $CdFe_2O_4$ sensor prepared by sol–gel method, Mater. Chem. Phys. 105 (2007) 67-70. https://doi.org/10.1016/j.matchemphys.2007.04.038.

[26] Bakuzis, A. F., Skeff, N. K., Gravina, P. P., Figueiredo, L. C., Morais, P. C., Magneto-optical properties of a highly transparent cadmium ferrite-based magnetic fluid, Appl. Phys. Lett. 84 (2004) 2355- 2357. https://doi.org/10.1063/1.1690497.

[27] Kaur, H., Singh, J., Randhawa, B. S., Essence of superparamagnetism in cadmium ferrite induced by various organic fuels via novel solution combustion method, Ceram. Int. 40 (2014) 12235-12243. https://doi.org/10.1016/j.ceramint.2014.04.067.

[28] Naseri, M. Optical and magnetic properties of monophasic cadmium ferrite ($CdFe_2O_4$) nanostructure prepared by thermal treatment method, J. Magn. Magn. Mater. 392 (2015) 107-113. https://doi.org/10.1016/j.jmmm.2015.05.026.

[29] Plocek, J., Hutlová, A., Niznanský, A., D., Bursık, J., Rehspringer, J.-L. Micka, Z. Preparation of $ZnFe_2O_4/SiO_2$ and $CdFe_2O_4/SiO_2$ nanocomposites by sol–gel method, J. Non-Cryst. Sol. 315 (2003) 70-76. https://doi.org/10.1016/S0022-3093(02)01595-8.

[30] Dippong , T., Cadar, O., Levei, E. A., Bibicu, I., Diamandescu, L., Leostean, C., Lazar, M., Borodi, G., Tudoran, L. B., Structure and magnetic properties of $CoFe_2O_4/SiO_2$ nanocomposites obtained by sol-gel and post annealing pathways, Ceram. Int. (2017) 2113-2122. https://doi.org/10.1016/j.ceramint.2016.10.192.

[31] Silva, J. B., Characterization of Porous Nanocomposites Formed by Cobalt Ferrites Dispersed in Sol-Gel Silica Matrix, J. Sol-Gel Sci. Technol. 35 (2015) 115–122. https://doi.org/10.1007/s10971-005-1378-1.

[32] Nalin, M., Poulain, M., Poulain, Mi., Ribeiro, S. J. L., Messaddeq, Y., Antimony oxide based glasses, J. Non-Cryst. Sol. 284 (2011) 110-116. https://doi.org/10.1016/S00223093(01)00388-X.

[33] Nečas, D., Klapetek, P., Gwyddion: an open-source software for SPM data analysis, Open Physics, 10 (1) (2011) 2391-5471. https://doi.org/10.2478/s11534-011-0096-2.

[34] Cullity, B. D., Stock, S. R., Elements of X Ray Diffraction, Prentice Hall, Upper Saddle River, New Jersey, 3rd ed., 2001.

Eclética Química Journal, vol. 43, n. 2, 2018, 32-43
ISSN: 1678-4618
DOI: 10.26850/1678-4618eqj.v43.2.2018.p32-43

[35] Tauc, J. Amorphous and Liquid Semiconductor. Plenum Publishing Company Ltd; New York, 1974.

[36] Miao, F., Deng, Z., LV, X., Gu, G., Wan, S., Fang, X., Zhang, Q., Yin, S., Fundamental properties of $CdFe_2O_4$ semiconductor thin film, Solid State Commun. 150 (2010) 2036–2039. https://doi.org/10.1016/j.ssc.2010.08.010.

[37] Shi, W., Liu, X., Zhang, Wang, Q., Zhang, L. Magnetic nano-sized cadmium ferrite as na efficient catalyst for the degradation of Congo red in the presence of microwave irradiation. RSC adv. 5 (2015) 51027-51034. https://doi.org/10.1039/C5RA07591B.

[38] Navarro, J. M. F., El Vidrio, CSIC Press, Madrid, Spain, 3rd ed., 2003.

[39] Siqueira, F. R. Preparação de vidros e vitrocerâmicas contendo metais de transição. Dissertação (Mestrado em Química) – Instituto de Química, Universidade Federal de São Carlos, São Carlos. 2014.

[40] Ganjoo, A., Gollovchak, R., Computer program PARAV for calculating optical constants of thin films and bulk materials: Case study of amorphous semiconductors, J. of Optoel. and adv. Mat. 10 (2008) 1328-1332.

Eclética Química Journal, vol. 43, n. 2, 2018, 32-43
ISSN: 1678-4618
DOI: 10.26850/1678-4618eqj.v43.2.2018.p32-43